First-principles calculations of clean Au(110) surfaces and chemisorption of atomic oxygen

M. Landmann, E. Rauls, and W. G. Schmidt
Lehrstuhl für Theoretische Physik, Universität Paderborn, 33095 Paderborn, Germany
(Received 5 August 2008; revised manuscript received 11 November 2008; published 15 January 2009)

We present detailed density-functional theory studies of the structures of clean Au(110) surfaces and the energetics of various atomic oxygen coverages. Various $(1\times r)$ "missing row" reconstructions of the clean Au(110) surface have been investigated. The surface energies of the clean reconstructed surfaces are found to be very close with an energy minimum for Au(110)-(1×3). The (111) microfacets formed at Au(110)-$(1\times r)$ reconstructed surfaces with $r>1$ allow further adsorption sites. Adsorption in pseudothreefold-coordinated sites, along close-packed rows in the topmost gold layer, is favored over other adsorption sites. On Au(110)-$(1\times r)$, adsorption energies are generally higher for these sites.

DOI: 10.1103/PhysRevB.79.045412 PACS number(s): 68.35.B−, 68.43.Bc, 68.43.Fg, 71.15.Nc

I. INTRODUCTION

Historically, the noble-metal gold was regarded as the embodiment of chemical inertness. The fact that gold does not oxidize in air and the small number of existing gold oxides show the low affinity of oxygen toward gold. While this behavior is a desired property for jewelry, nonoxidizing contacts in electronic industries, and medical uses such as dentistry, it hinders certain technical/chemical applications. Gold was even characterized as "catalytically dead."[1] On the other hand, interest in gold catalysis has been fueled by findings that (supported) nanometer-sized gold particle catalysts can be highly active in the field of low-temperature carbon monoxide oxidation as well as other catalytic reactions, such as hydrochlorination of acetylene (ethyne).[2,3] Haruta *et al.*[4] were the first to show that gold, supported by various metal oxides, catalyzes CO oxidation even for temperatures as low as 70 K. Especially gold supported on TiO_2, α-Fe_2O_3, and Co_3O_4 was shown to be very active low-temperature catalysts.[5]

This raises the question of how the oxygen molecule is activated and what is the nature of the various preliminary and/or intermediate Au-O complexes involved in these reactions. To accomplish a satisfactory theoretical understanding of catalytic properties[6] of gold at the fundamental level, not only the oxygen interaction with free or oxide supported gold nanoparticles/clusters[6–11] has been investigated but also the oxygen and CO (Refs. 12–14) interaction with Au single-crystal surfaces became a field of interest.

While oxygen chemisorption has been observed in the presence of surface impurities,[15,16] no dissociative oxygen chemisorption on clean extended monocrystal surfaces of gold has been observed in recent studies. Earlier investigations of oxygen interaction with gold single-crystal surfaces sometimes have shown contradictory results (see Ref. 17 and references therein). Sault *et al.*[18] studied O_2 adsorption on the Au(110)-(1×2) (missing row reconstructed) surface by applying pressures up to 1400 Torr and temperatures between 300 and 500 K. Under no circumstances any dissociative adsorption of O_2 was observed by thermal-desorption spectroscopy (TDS). This was confirmed by Gottfried *et al.*,[19] who pointed out that no desorption of O_2 is observable in TDS above 60 K after adsorption of oxygen on the surface under UHV conditions at a sample temperature of 28 K. This excluded a partial spontaneous conversion of physisorbed into chemisorbed oxygen.

To overcome the high activation barrier to produce a chemisorbed oxygen species, different methods including thermal dissociation,[18,20] oxygen-ion sputtering,[21] microwave discharge,[22] and the usage of reactive molecules such as NO_2 or O_3 (Ref. 23) have been reported so far. Gottfried *et al.*[19,24,25] produced chemisorbed oxygen on Au(110)-(1×2) by electron bombardment of physisorbed layers of oxygen molecules. The oxygen species, produced in that way, is characterized by a single TDS desorption state above 500 K, with second-order desorption kinetics at low coverages indicating chemisorbed oxygen atoms.

The Au(110) surface used in these studies features a characteristic missing row structure at room temperature. As established by diffraction techniques[26,27] and scanning tunneling microscopy (STM),[28,29] every second close-packed atomic row in the topmost atomic layer is missing in this surface reconstruction, resulting in a doubled periodicity in the [001] direction with respect to the structurally relaxed unreconstructed bulk truncated surface configuration Au(110)-(1×1). Every surface trench formed upon reconstruction consists of two (111) microfacets. The Au(110)-(1×2) surface is known to undergo two phase transitions—on one hand an Ising transition at $\approx$650 K, in which the surface deconstructs, and on the other hand a three-dimensional roughening transition at $\approx$700 K,[30,31] coming along with the destruction of the two-dimensional surface arrangements.

Additionally, surface reconstructions with deeper trenches (missing atoms in the second layer) and (1×3) periodicity have been observed on clean surfaces[26,28] and shown to be stable up to 350 K.[26] Furthermore, the appearance of a (1×3) reconstruction was observed to occur upon Cs (Ref. 32) or Ca adsorption.[33] Deeper corrugations than Au(110)-(1×3) have not been observed yet.[28] Also (1×3) steps on Au(110) can be stable up to temperatures as high as 500 K, as confirmed by high-temperature STM results.[31] In the following we will present a systematic density-functional theory (DFT) study of the structure and energetics of clean as well as atomic oxygen-covered Au(110) surfaces.

II. METHODOLOGY

We have performed first-principles DFT calculations with the plane-wave-based Vienna *Ab initio* Simulation Package (VASP).[34] In general the Kohn-Sham equations were solved using the generalized-gradient exchange-correlation (xc) functional approximation proposed by Perdew and Wang [generalized-gradient approximation (GGA)-PW91].[35] The additional usage of the local-density approximation (LDA) according to Ceperley and Alder[36] as parametrized by Perdew and Zunger[37] was explicitly mentioned in the text. The electron-ion interaction was described by the projector-augmented wave (PAW) method.[38,39] In the PAW data scalar relativistic corrections are contained. Throughout this work an energy cutoff of 400 eV was used to expand the wave functions into the plane-wave basis. The Brillouin-zone integration was performed using a cell-size-dependent Monkhorst-Pack k point sampling.[40] Thereby calculations in (4×4) surface unit cells (SUCs) are performed using a $(4\times4\times1)$ k-point mesh. For calculations with other SUC sizes, the k-point sets were chosen to have approximately the same k-point density. Thereby the first-order Methfessel-Paxton smearing method with a width of 0.2 eV was used. For gas-phase calculations of atomic and molecular oxygen only the Γ point was used.

If not stated otherwise, the surface slabs were modeled with eight layers of metal atoms. The vacuum region ($\sim$11.8 Å) was chosen to correspond to eight layers of bulk material. The atoms of the two bottom layers of the surface slab were kept fixed in their ideal bulk positions during the geometry relaxation. The positions of the gold atoms in the top six atomic layers were optimized without any constraint until forces on the atoms were less than 0.01 eV/Å. The dipole moment induced by the asymmetric slab geometry with different upper and lower surfaces was taken into account by applying a dipole correction in the z direction. For the potential-energy surface (PES) calculations, the oxygen atom was positioned on the points of an equidistant grid parallel to the surface, constraining its relaxation to the z direction. The positions of gold atoms in the top six layers and the oxygen atoms in z direction were relaxed until forces on them were less than 0.03 eV/Å. The methodology and numerical parameters of the present calculations are thus very similar to related studies.[41–44]

For consistency, all SUCs used here (cf. Fig. 1) are denoted by an integer multiple $(n\times m)$, $n,m=1,2,\ldots$ of the smallest SUC of the Au(110)-(1×1) surface, which is spanned by the two vectors $\vec{a}_1$ and $\vec{a}_2$, as shown in Fig. 4(a). The different oxygen coverages studied in this work are realized by placing one oxygen atom in the various SUCs shown in Fig. 1 that obey periodic boundary conditions.

Au(110) surface energies (at zero temperature) are calculated via

$$\sigma_{\text{surf}}^{1\times r}=\frac{1}{2A_{1\times r}}[E_{\text{tot}}^{1\times r}(N_{\text{Au}})-N_{\text{Au}}E_{\text{Au,bulk}}] \tag{1}$$

with $r=1,2,\ldots$ Here $E_{\text{tot}}^{1\times r}$ is the total energy of the periodically repeated surface unit cell of the $(1\times r)$-reconstructed surface, $N_{\text{Au}}^{1\times r}$ is the number of gold atoms in this unit cell,

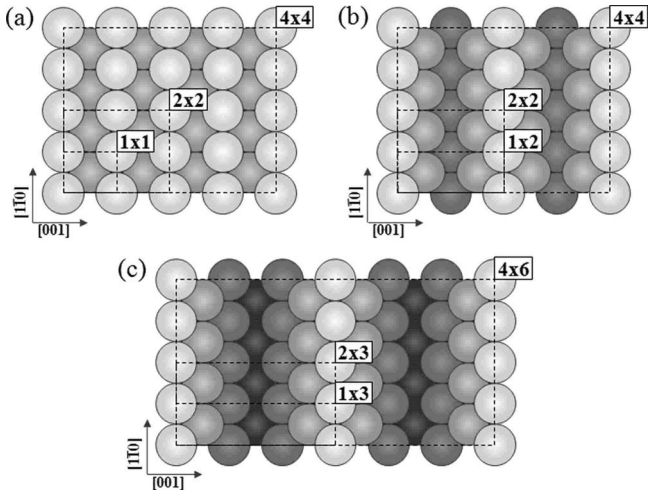

FIG. 1. Schematic top views of the geometric shape of (a) the unreconstructed Au(110)-(1×1) and the reconstructed missing row type surfaces (b) Au(110)-(1×2) and (c) Au(110)-(1×3). White circles correspond to first-layer gold atoms. Darker gray colors indicate gold atoms in deeper layers.

and $E_{\text{Au,bulk}}$ is the chemical potential of bulk Au atoms. Adsorption energies are defined as an average over all oxygen atoms in the considered surface unit cell through

$$E_{\text{ad}}^{1\times r}=-\frac{1}{N_{\text{O}}}[E_{\text{tot}}^{1\times r}(N_{\text{Au}},N_{\text{O}})-E_{\text{sub}}^{1\times r}(N_{\text{Au}})]+E_{\text{O}}-\frac{1}{2}E_{b,\text{O}_2}. \tag{2}$$

Here, $E_{\text{tot}}^{1\times r}$ is the total energy of the whole system containing N_{Au} gold atoms and N_{O} oxygen atoms. $E_{\text{sub}}^{1\times r}$ is the total energy of the relaxed substrate containing the same number of gold atoms, and E_{O} is the total energy of a free oxygen atom. By subtracting half the binding energy E_{b,O_2} of the gas-phase oxygen molecule, the adsorption energy is per definition given relative to molecular oxygen as the oxygen ground-state energy reference. Adsorption energies in terms of the foregoing definition describe a stable (exothermic) adsorption process in case of positive sign and an unstable (endothermic) process in case of negative sign.

To analyze the nature of the Au-O bond, we considered charge-density differences

$$\Delta n(\mathbf{r})=n_{\text{tot}}(\mathbf{r})-n_{\text{ad}}(\mathbf{r})-n_{\text{sub}}(\mathbf{r}), \tag{3}$$

which give insight in regions of electron accumulation and depletion. Thereby n_{tot} and $n_{\text{ad}}/n_{\text{sub}}$ are the valence electron densities of the relaxed adsorbate-substrate system and the adsorbate or substrate subsystem in the same position as in the total adsorbate-substrate system, respectively

III. RESULTS

A. Reference values

Within GGA-PW91, the calculated Au equilibrium lattice constant is $a_0=4.176$ Å (4.063 Å in LDA). The bulk modulus is $B_0=127$ GPa (186 GPa in LDA), and the cohesive energy per Au atom is 3.17 eV (4.38 eV in LDA). The cor-

responding experimental values are a_0=4.078 Å,[46] B_0 =172 GPa,[46] and 3.81 eV for the cohesive energy per Au atom.[48] The comparison confirms the typical finding that GGA (LDA) tends to underestimate (overestimate) chemical bond strengths.

The O_2 molecule bond length calculated in GGA is r_0 =1.24 Å and the corresponding vibrational frequency is ω_0 =1556 cm^{-1}. The binding energy per atom of a free oxygen molecule is $1/2E_{b_{O_2}}$=3.08 eV (spin-polarized calculation). Experimentally, values of ω_0=1580 cm^{-1}, r_0=1.21 Å,[47] and $1/2E_{b_{O_2}}$=2.56 eV (Ref. 49) are reported.

B. Au(110) surface geometry

We investigated unreconstructed and missing row type reconstructed Au(110) surfaces. In the predominantly observed Au(110)-(1×2) surface, one close-packed atomic row in the $[1\bar{1}0]$ direction in the topmost/first layer is missing. Higher $(1\times r)$ missing row type reconstructed surfaces can be created by removing $(r-n)$ close-packed rows from the nth atomic layer for $n=1,2,\ldots,(r-1)$.

Schematic top and side views of the clean Au(110)-(1×1) surface and the missing row type reconstructed Au(110)-(1×2) and Au(110)-(1×3) surfaces are pictured in Figs. 1 and 2. The structural parameters defined in Fig. 2 and summarized in Table I describe characteristic relaxations for unreconstructed and reconstructed surfaces. The unreconstructed surface features an alternating (+,−,+,−) contraction and expansion of interplanar distances Δd_{ij}. The largest change in interplanar distance is the contraction Δd_{12} between the topmost layers, which equals 12.9% of the bulk interplanar distance. Both missing row type reconstructed surfaces show a significantly increased inward relaxation of the topmost atomic layer compared to the (1×1) reconstruction. The interplanar distance contracts by about 21.7% and 23.0% for (1×2) and (1×3) reconstructions, respectively. The general trend of an inward relaxation of the first-layer atoms of metal surfaces was described by Finnis and Heine[50] based on Smoluchowski smoothing.[51] The missing atoms in the topmost atomic layer of the Au(110)-(1×2) surface cause a small buckling b_3 of 0.35 Å in the third as well as small lateral displacements in the second layer (p_2 =0.04 Å) and in the fourth layer (p_4=0.07 Å). The latter are often called pairing. As expected, the stronger roughness of the (1×3)-reconstructed Au(110) surface results in larger interplanar distance changes between lower-lying atomic layers. In addition to the lateral displacements in the second and the fourth layers, which are comparable to Au(110)-(1×2), the Au(110)-(1×3) surface shows a marginal pairing of third-layer atoms. The calculated structural parameters for Au(110)-(1×2) agree well with the available experimental data, in particular with low-energy electron diffraction (LEED) and x-ray results; cf. Table I.

C. Au(110) surface energy

In the present study both the (1×2)- and (1×3)-reconstructed Au(110) surfaces give rise to lower surface energies than the Au(110)-(1×1) surface. The surface

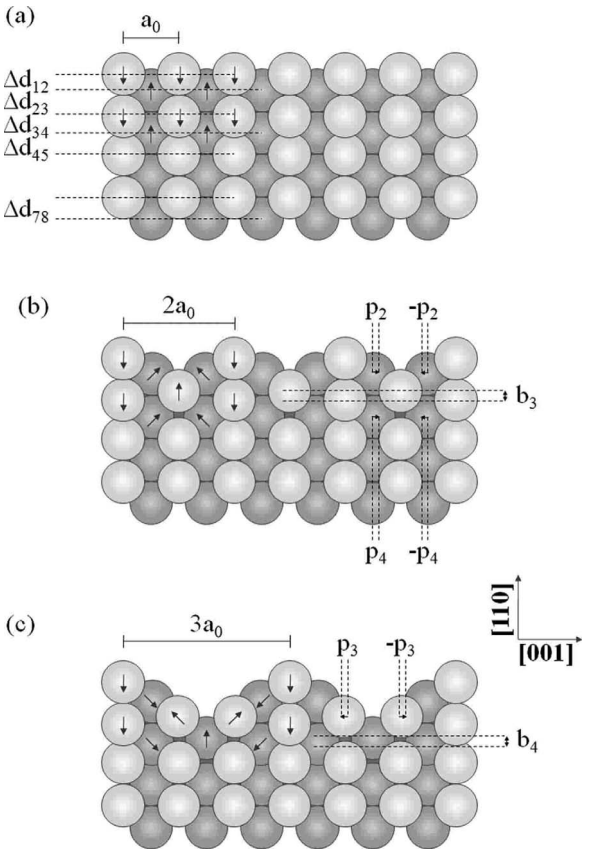

FIG. 2. Schematic side views of the geometric shape of (a) the unreconstructed Au(110)-(1×1) and the reconstructed missing row type surfaces (b) Au(110)-(1×2) and (c) Au(110)-(1×3). The calculated values for the defined structural parameters [contraction and expansion of interplanar distances Δd_{ij}, buckling b_k, and pairing (p_l)] are given in Table I. The arrows indicate atom displacements in the optimized surface structures with respect to atom positions in truncated bulk configuration.

energy sequence $\sigma_{surf}^{(1\times1)}>\sigma_{surf}^{(1\times2)}>\sigma_{surf}^{(1\times3)}$ does not change if slabs with 12 layers or symmetric slabs with 15 atomic layers are used; cf. Table II. However, the energy difference between the (1×2)- and (1×3)-reconstructed Au(110) surfaces is very small, less than 1 meV/Å^2 [more descriptively, this equals 12.34 meV per (1×1) unit cell]. We probed the influence of the xc functional and found that using the PBE[53] instead of the PW91 functional of the GGA changes the surface energies by less than 1 meV/Å^2. LDA calculations are found to result in significantly larger surface energies. However, they do not change the energetical order of the reconstructions obtained in GGA; cf. Table III.

Also contained in Table III are our results for $(1\times r)$ missing row type reconstructed surfaces up to r=6. The Au(110)-(1×3) surface is energetically most favored. However, $(1\times r)$ surfaces with $r>3$ are very close in energy and slightly more favorable than the (1×2) reconstruction. GGA and LDA surface energies differ by about ≈32.5 meV/Å^2.

We repeated the surface energy calculations for Au(110)-(1×1) and Au(110)-(1×2) using PAW potentials without scalar relativistic corrections (nonrelativistic lattice constant: a_0=4.439 Å). The reconstruction energy $\sigma_{rec}^{1\rightarrow2}$ is

TABLE I. Comparison of structural parameters as defined in Fig. 2 for the optimized surface geometries of the unreconstructed Au(110)-(1×1) surface and the two missing row type surface reconstructions Au(110)-(1×2) and Au(110)-(1×3). All structural parameters are given in angstroms. The changes in interplanar distances Δd_{ij} are given with respect to the bulk interplanar distance $\Delta d_{\mathrm{bulk}}=1.48$ Å and also calculated as a percentage of this value.

	Current DFT study					
	(1×1)		(1×2)		(1×3)	
Δd_{12} (Å) (%)	−0.19	(−12.9)	−0.32	(−21.7)	−0.34	(−23.0)
Δd_{23} (Å) (%)	0.13	(8.8)	0.03	(2.0)	0.03	(2.0)
Δd_{34} (Å) (%)	−0.05	(−3.4)	0	(0)	−0.17	(−11.5)
Δd_{45} (Å) (%)	0.04	(2.7)	0.03	(2.0)	0.14	(9.5)
p_2 (Å)			0.04		0.07	
p_3 (Å)					0.01	
p_4 (Å)			0.07		0.07	
b_3 (Å)			0.35		0.32	
b_4 (Å)					0.37	

	Experimental results (Ref. 45) for Au(110)-(1×2)					
	LEED	LEED	LEIS	LEIS	MEIS	X-ray
Δd_{12} (Å)	−0.22	−0.29	−0.20	−0.15	−0.26	−0.32
Δd_{23} (Å)		0.03			0.06	
Δd_{34} (Å)						
Δd_{45} (Å)						
p_2 (Å)		0.07	<0.1	0	<0.1	0.05
p_3 (Å)						
p_4 (Å)						0.05
b_3 (Å)		0.24			0.20	
b_4 (Å)						

drastically reduced from −2.28 to −0.05 meV/Å^2 but does not change its sign. The corresponding nonrelativistic surface energies are $\sigma_{\mathrm{surf}}^{(1\times1)}=45.85$ meV/Å^2 and $\sigma_{\mathrm{surf}}^{(1\times2)}=45.80$ meV/Å^2.

D. Oxygen adsorption

We started our investigations of oxygen-covered gold surfaces by calculating the PES for oxygen atoms adsorbed on Au(110)-(1×r) with $r=1$, 2, and 3; see Fig. 3. All calculations concerning oxygen adsorption were done using the PW91 xc functional.

With the exception of the $M0$ adsorption energy maximum on Au(110)-(1×1), all maxima correspond to threefold-coordinated sites on (111) microfacets of the surface trenches. $M1,\ldots,M5$ represent *pseudothreefold* (PT) (cf. Fig. 4) adsorption sites. Deeper trench sites are energetically less favorable. The PT1 sites located along the topmost close-packed atomic rows for the two missing row type reconstructed surfaces yield the highest adsorption energy; cf. Table IV. In these sites, the oxygen atom forms two bonds to first-layer atoms and one bond to a second-layer atom. In PT2 sites (corresponding to M2 in Fig. 3), the oxygen binds to one first-layer and two second-layer Au atoms. Like this, all oxygen atoms in odd numbered PT sites show two bonds to the upper adjacent layer atoms and one bond to the lower adjacent layer atoms, and vice versa for even numbered sites.

TABLE II. Surface energies σ_{surf} of (1×r) surfaces for $r=1$, 2, and 3 in meV/Å^2 and reconstruction energies $\sigma_{\mathrm{surf}}^{1\to r}$.

	$\sigma_{\mathrm{surf}}^{(1\times1)}$	$\sigma_{\mathrm{surf}}^{(1\times2)}$	$\sigma_{\mathrm{surf}}^{(1\times3)}$	$\sigma_{\mathrm{rec}}^{1\to2}$	$\sigma_{\mathrm{rec}}^{1\to3}$
8 layer, asymmetric	58.05	55.77	54.83	−2.28	−3.22
12 layer, asymmetric	58.39	56.12	55.29	−2.27	−3.10
15 layer, symmetric	56.61	51.80	50.98	−4.81	−5.63

TABLE III. Surface energies $\sigma_{\mathrm{surf}}^{1\times r}$ in meV/Å^2 and corresponding reconstruction energies $\sigma_{\mathrm{surf}}^{1\to r}$. Surface energies were calculated using $(8+r)$ layer slabs.

$(1\times r)$	$\sigma_{\mathrm{surf,GGA}}^{(1\times r)}$	$\sigma_{\mathrm{surf,LDA}}^{(1\times r)}$	$\sigma_{\mathrm{rec,GGA}}^{1\to r}$	$\sigma_{\mathrm{rec,LDA}}^{1\to r}$
(1×1)	57.68	90.33		
(1×2)	55.14	87.52	−2.54	−2.81
(1×3)	54.65	87.07	−3.03	−3.26
(1×4)	54.68	87.14	−3.00	−3.19
(1×5)	54.74	87.26	−2.94	−3.19
(1×6)	54.83	87.38	−2.85	−2.95

Based on these findings, we investigated various coverages for the different pseudothreefold sites within the surface trenches. Thereby we considered the highly symmetric adsorption sites *short bridge* (SB), *long bridge* (LB), *top* (TP), and *hollow* (HL). The adsorption energies, calculated using Eq. (2) with reference to the free oxygen molecule, are summarized in Table IV.

The TP site is energetically the least favorable position followed by the HL sites. For adsorption in HL or LB position, energies decrease with stronger surface reconstructions. Some SB and PT sites show positive values of E_{ad} for lower coverages. These adsorption energies are very small in case of SB sites. Only the adsorption in pseudothreefold sites, along the topmost close-packed atomic rows, shows significant positive adsorption energies E_{ad} between 150 and 350 meV.

For the highest considered oxygen coverages, E_{ad} never becomes positive. The adsorption energies of most adsorption sites clearly show the lowest values for these high oxygen coverages. This behavior is most obvious for SB and PT1 sites.

Table V summarizes the bond lengths for the lowest considered oxygen coverages of Au(110)-$(1\times r)$. These low coverages can be seen as a realization of a single oxygen atom on the surface, as we will discuss in Sec. IV. The bond lengths almost show no dependence on the surface reconstruction for adsorption in TP (1.90 Å) or SB (2.04 Å) sites. Adsorption in PT1 sites differs for the unreconstructed and the reconstructed surfaces. In the case of adsorption in HL and LB sites, we find ambiguous changes in the Au-O bond lengths for the different reconstructions.

To gain insight into the electronic structure of the Au-O bond, we have calculated charge-density differences using Eq. (3). These charge-density differences are illustrated for the three different coverages on Au(110)-(1×2) in Fig. 5. The gold atoms bonded to the oxygen atom show an electron depletion and a charge transfer from the 5*d*-like Au orbitals toward the oxygen atom. There is a charge accumulation close to the center of the three Au-O bonds, which is characteristic for a covalent bond. A charge polarization at the oxygen atom can be seen with a region of electron depletion

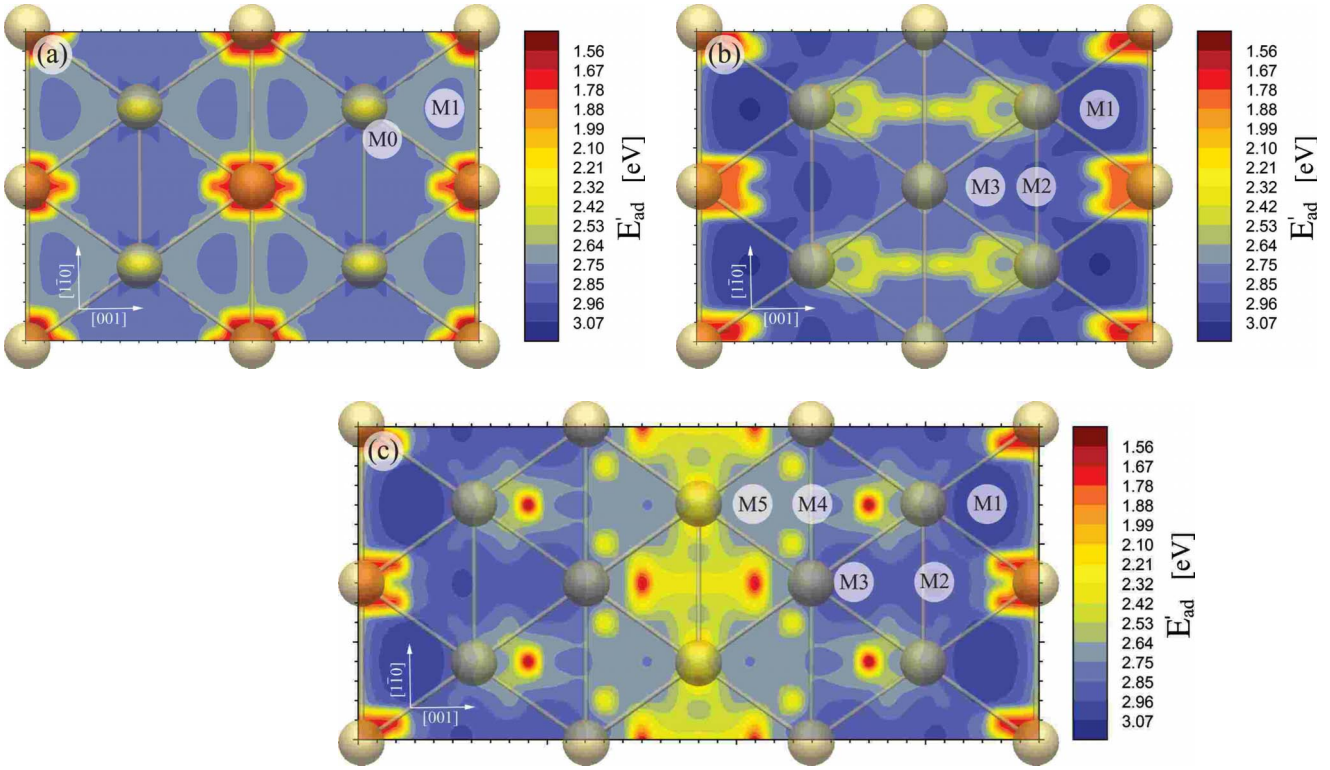

FIG. 3. (Color online) Potential-energy surfaces of (a) the O/Au(110)-(1×1) surface ($\Theta=0.081$ Å^{-2}, 2×2 SUC), (b) the missing row-reconstructed O/Au(110)-(1×2) surface ($\Theta=0.041$ Å^{-2}, 2×2 SUC), and (c) the missing row type reconstructed O/Au(110)-(1×3) surface ($\Theta=0.027$ Å^{-2}, 2×3 SUC). The SUCs are defined in Fig. 1. The adsorption energies $E'_{\mathrm{ad}}=E_{\mathrm{ad}}+\frac{1}{2}E_{b,\mathrm{O}_2}$, related to atomic oxygen, calculated for 35 sites in the case of Au(110)-(1×1), for 65 sites in the case of Au(110)-(1×2), and for 95 sites in the case of Au(110)-(1×3) are color coded. Local adsorption energy maxima are denoted by $M0, M1, \ldots, M5$.

TABLE IV. Adsorption energies E_{ad} (meV) for various oxygen coverages of Au(110)-(1×1), Au(110)-(1×2), and Au(110)-(1×3). (TP: top; SB: short bridge; LB: long bridge; HL: hollow; PT: pseudo-threefold; cf. Fig. 4). Per definition negative adsorption energies describe an unstable (endothermic) process and positive energies describe a stable (exothermic) process.

		Adsorption energy E_{ad} (meV)						
Coverage (Å^{-2})		0.081	0.041	0.027	0.020	0.014	0.005	0.003
HL	(1×1)	−756	−277		−355			
TP	(1×1)	−1402	−924		−896			
LB	(1×1)	−253	−280		−181			
SB	(1×1)	−456	23		69			
PT1	(1×1)	−331	156		172			
HL	(1×2)		−365		−641		−648	
TP	(1×2)		−1316		−1034		−911	
LB	(1×2)		−539		−662		−578	
SB	(1×2)		−449		−32		25	
PT1	(1×2)		−8		331		328	
PT2	(1×2)		−98		−66		−123	
PT3	(1×2)						−246	
HL	(1×3)			−603		−727		−734
TP	(1×3)			−1344		−1048		−918
LB	(1×3)			−729		−624		−584
SB	(1×3)			−473		−34		21
PT1	(1×3)			−23		342		349
PT2	(1×3)			−110		−64		−53
PT3	(1×3)			−141		−25		10
PT4	(1×3)			−312		−218		43
PT5	(1×3)			−337		−253		−246

pointing toward the surface and a region of electron accumulation pointing in the opposite direction.

IV. DISCUSSION

The findings described in Sec. III require the discussion of two main aspects: on one hand, the relevance of surface energies for the formation of surface reconstructions, and on the other hand the characteristic properties of oxygen chemisorption on Au(110)-$(1\times r)$ surfaces.

A. Clean surface energies

In Sec. III, we have shown that the Au(110) surface reduces its surface energy by forming the (1×2)-periodic missing row reconstruction. Furthermore, all higher-order $(1\times r)$, $r>2$, missing row type reconstructions up to $r=6$ show even lower surface energies than Au(110)-(1×2) (cf. Table III) and are very close in energy (±0.2 meV/Å^2 for GGA), thus indicating a very shallow potential-energy surface.

The only significant difference of surface energies affects the unreconstructed-reconstructed transition of (1×1) to (1×2). Changes in the surface energies of the differently reconstructed surfaces result from the energy gain due to the formation of larger close-packed (111) microfacets and the energy loss due to the larger number of surface atoms, i.e., the larger number of bonds to be broken during creation of the particular surface. Since the surface energies of $(1\times r)$ surfaces $(r>2)$ vary only slightly, these contributions cancel out each other nearly independently from the particular order of the missing row reconstruction.

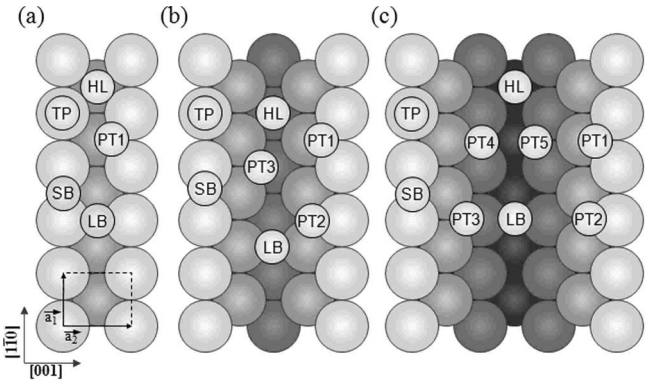

FIG. 4. Definition of adsorption sites on (a) the unreconstructed Au(110)-(1×1) and the reconstructed missing row type surfaces; (b) Au(110)-(1×2); and (c) Au(110)-(1×3) (TP: top; SB: short bridge; LB: long bridge; HL: hollow; PT: pseudothreefold).

TABLE V. Au-O bond lengths of adsorbed atomic oxygen on the Au(110)-$(1\times r)$, $r=1$, 2, and 3 surfaces. The values correspond to $\Theta=0.005$ Å^{-2} for Au(110)-(1×1) and Au(110)-(1×2) and to $\Theta=0.003$ Å^{-2} for Au(110)-(1×3). As described in text, these coverages correspond to single oxygen atom on the various SUCs.

		Au-O bond length(Å)			
Site	Surface	1st layer	2nd layer	3rd layer	4th layer
HL	(1×1)	2.46	2.29		
TP	(1×1)	1.90			
LB	(1×1)	2.08			
SB	(1×1)	2.04			
PT1	(1×1)	2.11	2.32		
HL	(1×2)		2.44	2.23	
TP	(1×2)	1.90			
LB	(1×2)		2.17	2.33	
SB	(1×2)	2.04			
PT1	(1×2)	2.13	2.19		
PT2	(1×2)	2.14	2.15		
PT3	(1×2)		2.12	2.23	
HL	(1×3)			2.51	2.21
TP	(1×3)	1.90			
LB	(1×3)			2.21	2.33
SB	(1×3)	2.04			
PT1	(1×3)	2.13	2.19		
PT2	(1×3)	2.14	2.15		
PT3	(1×3)		2.14	2.23	
PT4	(1×3)		2.11	2.16	
PT5	(1×3)			2.21	2.13

The Au(110)-(1×3) surface has been found to represent the absolute minimum. The fact that at no time the sequence of surface energies was found to change (cf. Tables II and III), regardless of the calculational setup, largely rules out the sequence to be a numerical or methodological artifact. That the surface energies of higher missing row type reconstructions are very close in energy has already been shown by the early calculations of Garofalo *et al.*,[52] who performed molecular dynamics using an empirical many-body force "glue" Hamiltonian. However, in these calculations, the (1×2) surface was found to be the lowest energy surface. Guillopè and Legrand[54] concluded from a simple tight-binding scheme that the (1×3) surface represents the energetical minimum among the $(1\times r)$ surfaces with $r=1,\ldots,9$. Bohnen and Ho[55] were the first to report surface energies based on first-principles total-energy calculations. They found a slab-thickness dependence of the (1×2)-(1×3) surface energy sequence. For seven layer slabs, separated by three layers of vacuum, the (1×2) surface had lower surface energy than the (1×3) surface. This sequence was found to invert for eleven layers, also separated by three layers of vacuum. As apparent from the data summarized in Ref. 56, the energetical ordering of (1×2) and (1×3) surfaces seems ambiguous. This is probably related to the very small energy differences and the fact that the calculation of surface energies is very sensitive to the value of E_{bulk}. The large bandwidth of energies reported in the literature, that almost covers 1 order of magnitude, strongly limits the comparability of surface energies calculated on different theoretical levels.

So far, the discussion of the surface energy ordering was only based on the zero-temperature limit of the underlying theoretical methodology. In order to consider the experimentally relevant case $T>0$ K, we calculated the vibrational entropy contributions for the (1×2)- and (1×3)-reconstructed surfaces. To this end, the normal modes were calculated as eigenvalues of the dynamical matrix of an eight layer slabs with the four lowest layers kept fixed (for details cf. Refs. 57–59). Based on this, temperature-dependent surface energies can be calculated via replacing the DFT total energy E_{tot} in Eq. (1) by the corresponding free energy $F=E_{\mathrm{tot}}-TS_{\mathrm{vib}}$.

The vibrational energy contributions turned out to be larger for the (1×2)-reconstructed surface. This leads to a temperature-dependent change in the stability order, which occurs at $T=112$ K. At room temperature ($T=300$ K), the calculated entropic energy difference between the (1×2)- and the (1×3)-reconstructed surfaces is $\Delta TS_{\mathrm{vib}}=5.4$ meV/Å^2. In agreement with experimental findings, the (1×2) reconstruction is, thus, stabilized over the (1×3) reconstruction at room temperature. This temperature dependence also explains the observation of both surface reconstructions in various experiments.

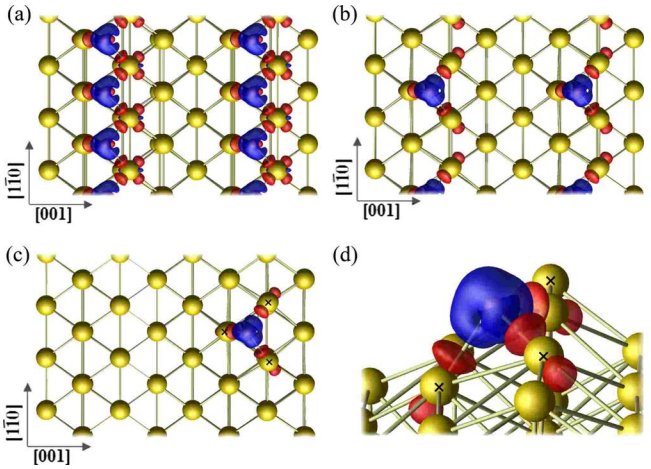

FIG. 5. (Color online) Charge-density difference plots (isosurface values: $\pm 0.055\ e/\text{Å}^3$) for oxygen in PT1 sites on the missing row-reconstructed Au(110)-(1×2) surface (4×4 SUC). Shown are the oxygen coverages (a) 0.041, (b) 0.020, and [(c) and (d)] 0.005 Å^{-2}. Marked atoms in (c) and (d) are equal. Blue color indicates regions of electron accumulation and red color indicates regions of electron depletion.

B. Trends in oxygen coverage of Au(110)-$(1\times r)$

The calculated adsorption energies show that oxygen chemisorption on Au(110)-$(1\times r)$ surfaces $(r=1,2,3)$ mainly occurs in pseudothreefold sites. Due to the missing row type induced reconstruction, this is consistent with the finding that oxygen adsorption on a Au(111) surface shows the highest adsorption energies for the threefold-coordinated fcc-hollow sites.[60] While the higher-order missing row type reconstruction allows adsorption in further pseudothreefold sites that represent local adsorption energy maxima (cf. Fig. 3), the PT1 sites, located along the topmost close-packed atomic rows, remain the most important adsorption sites. Adsorption sites located at the bottom of the surface trenches are increasingly unfavorable for the deeper trenches occurring in the case of the stronger surface reconstruction. This leads to the assumption that low-coverage oxygen adsorption will be very similar for O/Au(110)-(1×2) and O/Au(110)-(1×3).

Since PT1, PT3, PT4, and SB are the only sites with positive adsorption energies E_{ad} (at least for the lowest coverage), with respect to the free oxygen molecule and that E_{ad} is very small for adsorption in PT3, PT4, and SB sites, the following considerations mainly apply to adsorption in PT1 sites. As apparent from the charge-density difference plot for the Au(110)-(1×2) surface in Figs. 5(b) and 5(c), the Au-O interaction of the threefold-coordinated oxygen atoms is almost completely determined by its interaction with the three directly bonded Au-surface atoms. As a consequence, the adsorption energies for PT1 sites in Table IV vary only weakly for the lowest and second lowest coverages on all surfaces. Adsorption in PT1 sites can, thus, be regarded as the limiting case of a single isolated atom on the surface if every second PT1 site (or less) along a close-packed atomic row in the topmost layer is occupied. In this context, our lowest coverages clearly show the properties of one isolated oxygen atom on the surfaces under discussion.

In Fig. 5(a) the charge-density differences for O/Au(110)-(1×2) with a coverage of 0.041 Å^{-2} clarifies the reason for lower adsorption energies for the highest considered coverage. Due to occupation of every PT1 site along the [1$\bar{1}$0] direction, every first-layer Au atom is bonded to two oxygen atoms. Since the Au-O bond goes along with a charge transfer from the gold toward the oxygen atom, neighboring oxygen atoms constrict themselves indirectly by distributing charge from one Au atom to two oxygen atoms. Consequently, the adsorption energies E_{ad} become slightly negative at higher coverages $\Theta=0.041$ Å^{-2} on Au(110)-(1×2) and $\Theta=0.027$ Å^{-2} on Au(110)-(1×3) and significantly negative for $\Theta=0.081$ Å^{-2} on the unreconstructed Au(110)-(1×1) surface.

Compared to the ideal Au surface, oxygen adsorption is stabilized by a factor of 2 on the missing row reconstruction (cf. Table IV). The order of the missing row type surface reconstruction turned out to be less important because the adsorption energy difference for adsorption in every second PT1 site on the (1×2) and the (1×3) surfaces is very small; it amounts to only 21 meV. Correspondingly, the Au-O bond lengths of oxygen in PT1 sites have been calculated to be identical for adsorption on (1×2)- and (1×3)-reconstructed surfaces.

V. SUMMARY

In summary, we have shown that surface energies, calculated with a state-of-the-art DFT implementation, favor the (1×3) surface reconstruction of the Au(110) surface. Further higher-order missing row type reconstructions have been calculated to be very close in energy, thus indicating a very shallow potential-energy surface with a series of local $(1\times r)$-reconstructed minima of the clean Au(110) surface. A consideration of the vibrational entropy contributions leads to a stabilization of the (1×2)-reconstructed surface over the (1×3)-reconstructed surface at room temperature.

Our investigations of oxygen adsorption on missing row type reconstructed Au(110) surfaces show that the upper adsorption energy limit for adsorption of a single atoms on the Au(110) surfaces is $\approx$350 meV. This adsorption energy is only reached when the oxygen coverage does not exceed the occupation of every second PT1 site on a missing row type reconstructed surface. The missing row reconstruction has been found to have a significant effect on the stabilization of the oxygen chemisorption. The effect of the higher-order missing row type reconstruction [Au(110)-(1×3)] on the most stable adsorption sites, however, seems to be negligible.

ACKNOWLEDGMENTS

The calculations were done using grants of computer time from the Paderborn Center for Parallel Computing (PC^2) and the Höchstleistungs-Rechenzentrum Stuttgart. The Deutsche Forschungsgemeinschaft is acknowledged for financial support.

[1] A. Stephen K. Hashmi, Gold Bull. **37** (1-2), 51 (2004).
[2] G. J. Hutchings, Gold Bull. **29** (4), 123 (1996).
[3] G. J. Hutchings, Catal. Today **72**, 11 (2002).
[4] M. Haruta, T. Kobayashi, H. Sano, and N. Yamada, Chem. Lett. **16**, 405 (1987).
[5] M. Haruta, S. Tsubota, T. Kobayashi, H. Kageyama, M. J. Genet, and B. Delmon, J. Catal. **144**, 175 (1993).
[6] L. M. Molina and B. Hammer, Appl. Catal., A **291**, 21 (2005).
[7] G. Mills, M. S. Gordon, and H. Metiu, J. Chem. Phys. **118**, 4198 (2003).
[8] A. Franceschetti, S. J. Pennycook, and S. T. Pantelides, Chem. Phys. Lett. **374**, 471 (2003).
[9] L. M. Molina and B. Hammer, Phys. Rev. B **69**, 155424 (2004).
[10] L. M. Molina, M. D. Rasmussen, and B. Hammer, J. Chem. Phys. **120**, 7673 (2004).
[11] L. M. Molina and B. Hammer, J. Chem. Phys. **123**, 161104 (2005).
[12] J. M. Gottfried, K. J. Schmidt, S. L. M. Schroeder, and K. Christmann, Surf. Sci. **536**, 206 (2003).
[13] J. Michael Gottfried and K. Christmann, Surf. Sci. **566-568**, 1112 (2004).
[14] D. Loffreda and P. Sautet, J. Phys. Chem. B **109**, 9596 (2005).
[15] M. E. Schrader, Surf. Sci. **78**, L227 (1978).
[16] J. J. Pireaux, M. Chtaib, J. P. Delrue, P. A. Thiry, M. Liehr, and R. Caudano, Surf. Sci. **141**, 211 (1984).
[17] N. Saliba, D. H. Parker, and B. E. Koel, Surf. Sci. **410**, 270 (1998).
[18] A. G. Sault, R. J. Madix, and C. T. Campbell, Surf. Sci. **169**, 347 (1986).
[19] J. M. Gottfried, K. J. Schmidt, S. L. M. Schroeder, and K. Christmann, Surf. Sci. **511**, 65 (2002).
[20] N. D. S. Canning, D. Outka, and R. J. Madix, Surf. Sci. **141**, 240 (1984).
[21] J. M. Gottfried, N. Elghobashi, S. L. M. Schroeder, and K. Christmann, Surf. Sci. **523**, 89 (2003).
[22] Ch. Linsmeier and J. Wanner, Surf. Sci. **454-456**, 305 (2000).
[23] D. H. Parker and B. E. Koel, J. Vac. Sci. Technol. A **8**, 2585 (1990).
[24] J. M. Gottfried, K. J. Schmidt, S. L. M. Schroeder, and K. Christmann, Surf. Sci. **525**, 184 (2003).
[25] J. M. Gottfried, K. J. Schmidt, S. L. M. Schroeder, and K. Christmann, Surf. Sci. **525**, 197 (2003).
[26] W. Moritz and D. Wolf, Surf. Sci. **88**, L29 (1979).
[27] W. Moritz and D. Wolf, Surf. Sci. **163**, L655 (1985).
[28] G. Binnig, H. Rohrer, Ch. Gerber, and E. Weibel, Surf. Sci. **131**, L379 (1983).
[29] T. Gritsch, D. Coulman, R. J. Behm, and G. Ertl, Surf. Sci. **257**, 297 (1991).
[30] M. Sturmat, R. Koch, and K. H. Rieder, Phys. Rev. Lett. **77**, 5071 (1996).
[31] R. Koch, M. Sturmat, and J. J. Schulz, Surf. Sci. **454-456**, 543 (2000).
[32] P. Häberle, P. Fenter, and T. Gustafsson, Phys. Rev. B **39**, 5810 (1989).
[33] R. Michaelis and D. M. Kolb, Surf. Sci. **234**, L281 (1990).
[34] G. Kresse and J. Furthmüller, Comput. Mater. Sci. **6**, 15 (1996).
[35] J. P. Perdew, J. A. Chevary, S. H. Vosko, K. A. Jackson, M. R. Pederson, D. J. Singh, and C. Fiolhais, Phys. Rev. B **46**, 6671 (1992).
[36] D. M. Ceperley and B. J. Alder, Phys. Rev. Lett. **45**, 566 (1980).
[37] J. P. Perdew and A. Zunger, Phys. Rev. B **23**, 5048 (1981).
[38] P. E. Blöchl, Phys. Rev. B **50**, 17953 (1994).
[39] G. Kresse and D. Joubert, Phys. Rev. B **59**, 1758 (1999).
[40] H. J. Monkhorst and J. D. Pack, Phys. Rev. B **13**, 5188 (1976).
[41] M. Preuss, W. G. Schmidt, and F. Bechstedt, Phys. Rev. Lett. **94**, 236102 (2005).
[42] S. Blankenburg and W. G. Schmidt, Phys. Rev. B **74**, 155419 (2006).
[43] E. Rauls, S. Blankenburg, and W. G. Schmidt, Surf. Sci. **602**, 2170 (2008).
[44] E. Rauls and W. G. Schmidt, J. Phys. Chem. C **112**, 11490 (2008).
[45] A. Fasolino, A. Selloni, and A. Shkrebtii, in *Landolt-Börnstein - Group III Condensed Matter*, Vol. 24a, Physics of Solid Surfaces - Structure (Springer, New York, 1993).
[46] G. Chiarotti, in *Landolt-Börnstein - Group III Condensed Matter*, Vol. 24a, Physics of Solid Surfaces - Structure (Springer, New York, 1993).
[47] D. R. Stull and H. Prophet, *JANAF Thermochemical Tables*, 2nd ed. (1971).
[48] Ch. Kittel, *Einführung in die Festkörpertheorie*, 13.Auflage (Oldenbourg, München, Wien, 2002).
[49] K. P. Huber and G. Herzberg, *Constants of Diatomic Molecules*, Molecular Spectra and Molecular Structure Vol. IV (Van Nostrand Reinhold, New York, 1997).
[50] M. W. Finnis and V. Heine, J. Phys. F: Met. Phys. **4**, L37 (1974).
[51] R. Smoluchowski, Phys. Rev. **60**, 661 (1941).
[52] M. Garofalo, E. Tosatti, and F. Ercolessi, Surf. Sci. **188**, 321 (1987).
[53] John P. Perdew, Kieron Burke, and Matthias Ernzerhof, Phys. Rev. Lett. **77**, 3865 (1996).
[54] M. Guillopè and B. Legrand, Surf. Sci. **215**, 577 (1989).
[55] K.-P. Bohnen and K. M. Ho, Electrochim. Acta **40**, 129 (1995).
[56] A. Y. Lozovoi and A. Alavi, Phys. Rev. B **68**, 245416 (2003).
[57] E. Rauls and Th. Frauenheim, Phys. Rev. B **69**, 155213 (2004).
[58] B. Lange and W. G. Schmidt, Surf. Sci. **602**, 1207 (2008).
[59] M. Landmann, E. Rauls, and W. G. Schmidt, J. Phys. Chem. C (unpublished).
[60] H. Shi and C. Stampfl, Phys. Rev. B **76**, 075327 (2007).